Enhanced Photocatalytic and Antimicrobial Performance of a Multifunctional Cu-loaded Nanocomposite under UV light: Theoretical and Experimental Study

M. Abd Elkodous[a], Ahmed M. El-Khawaga[b,c], M. I. A. Abdel Maksoud[d], Gharieb S. El-Sayyad[e,†], Nurhaswani Alias[f], Hazem Abdelsalam[g,h], Medhat A. Ibrahim[i,j], Mohamed A. Elsayed[b], Go Kawamura[a], Zainovia Lockman[f], Wai Kian Tan[k], and Atsunori Matsuda[a,†]

[a] Department of Electrical and Electronic Information Engineering, Toyohashi University of Technology, 1-1 Hibarigaoka, Tempaku-cho, Toyohashi, Aichi 441-8580, Japan.

[b] Chemical Engineering Department, Military Technical College (MTC), Egyptian Armed Forces, Cairo, Egypt.

[c] Faculty of medicine, Galala University, Suez, Egypt.

[d] Materials Science Lab., Radiation Physics Department, National Center for Radiation Research and Technology (NCRRT), Atomic Energy Authority, Cairo, Egypt.

[e] Department of Microbiology & Immunology, Faculty of Pharmacy, Galala University, New Galala city, Suez, Egypt.

[f] School of Materials and Mineral Resources Engineering, Engineering Campus, Universiti Sains Malaysia, 14300, Nibong Tebal, Pulau Pinang, Malaysia.

[g] School of Materials Science and Engineering, Yancheng Institute of Technology, Yancheng 224051, P. R. China.

[h] Theoretical Physics Department, National Research Centre, El-Buhouth Str., Dokki, Giza, 12622, Egypt.

[i] Nanotechnology Research Centre (NTRC), The British University in Egypt (BUE), Suez Desert Road, El-Sherouk City, Cairo, 11837, Egypt

[j] Molecular Spectroscopy and Modeling Unit, Spectroscopy Department, National Research Centre, 33 El-Bohouth St., 12622, Dokki, Giza, Egypt

[k] Institute of Liberal Arts and Sciences, Toyohashi University of Technology, 1-1 Hibarigaoka, Tempaku-cho, Toyohashi, Aichi, 441-8580, Japan.

[†] Corresponding author.

1. Preparation of the composite matrix ($Co_{0.5}Ni_{0.5}Fe_2O_4/SiO_2/TiO_2$)

A layer-by-layer method was used in the preparation of the composite matrix employed in this study, the detailed steps of which are mentioned in previously published articles [1, 2] and are presented in **Fig. S. 1**, where the composite matrix is denoted as (CNFST).

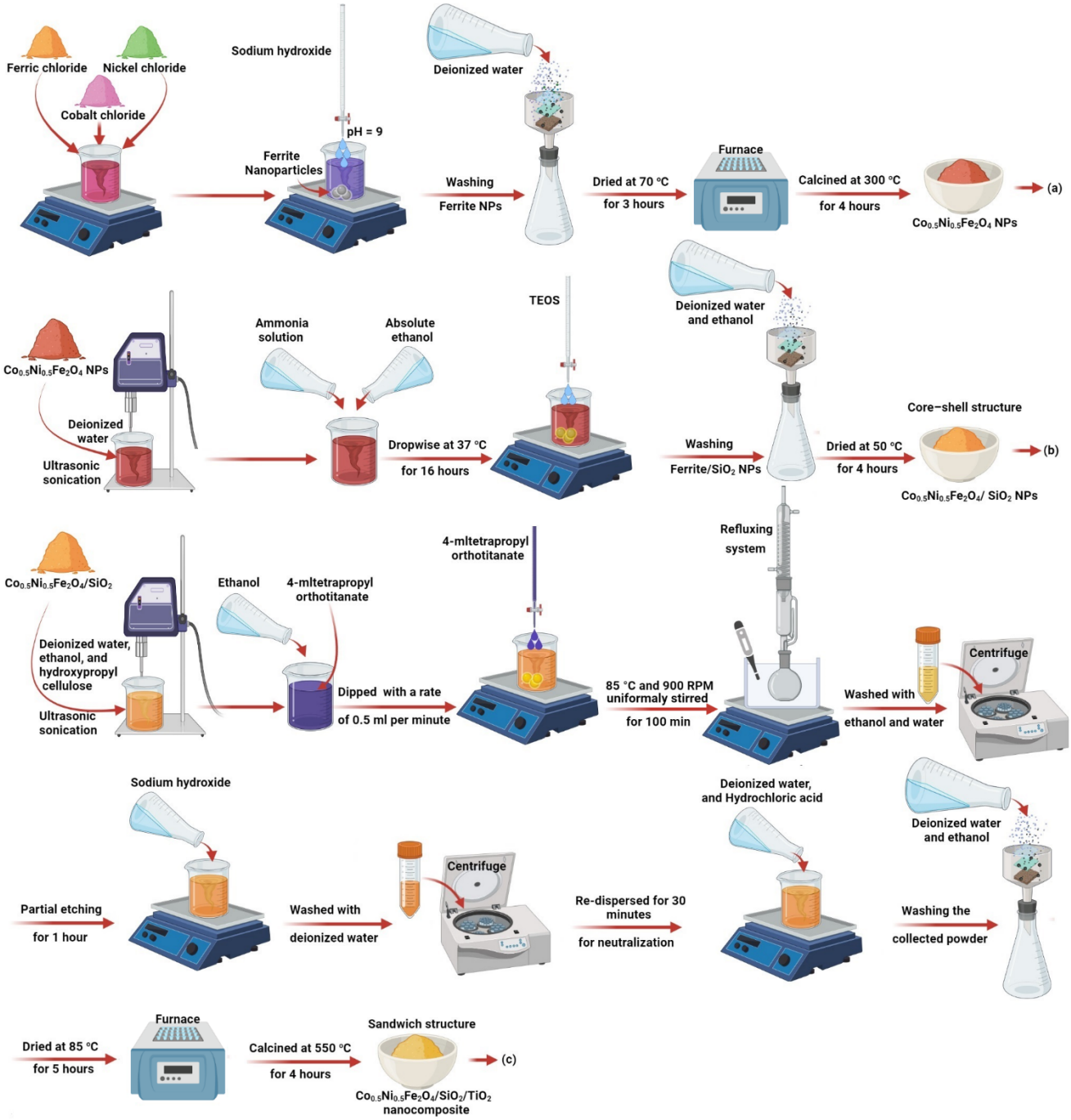

Fig. S. 1: Step-by-step preparation steps of CNFST nanocomposite.

2. Preparation of copper nanoparticles (Cu NPs)

Cu NPs were prepared using a modified hydrothermal method developed by Jia *et al.* [3] Briefly, ascorbic acid (6.8 g) was dissolved in deionized (DI) water (400 mL) under magnetic stirring for 10 min. Then, copper acetate monohydrate (0.8 g) was added to the above solution under constant stirring for a further 10 min at room temperature. After that, the reaction vessel was moved into a water bath and the temperature was increased to 90°C, after which the reaction was continued for 5 h. After this time, the carbon dot (C-dot)-containing supernatant was discarded, and the formed Cu precipitate was collected via centrifugation at 7000 rpm for 12 min. After that, the collected particles were washed several times using DI water. Finally, the washed particles were dried in vacuum for

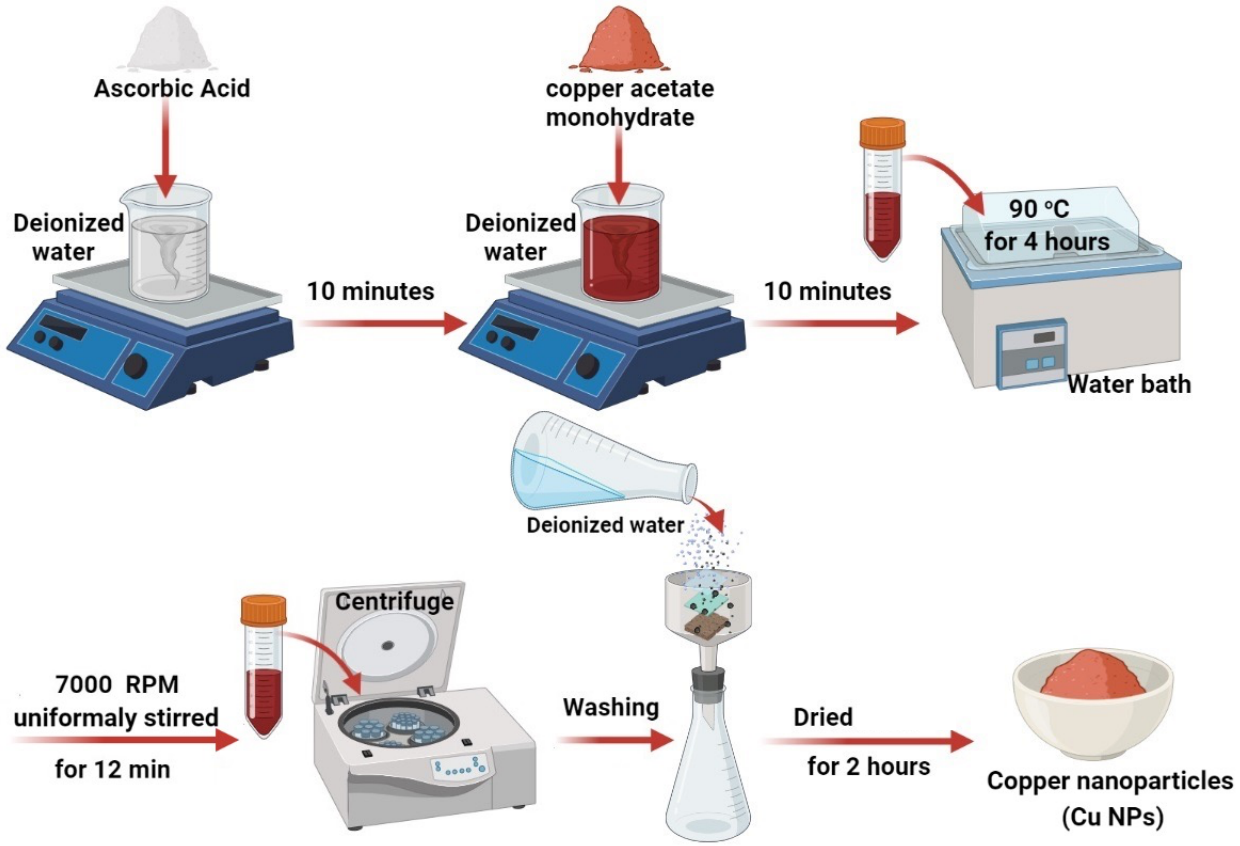

2 h in air, as shown in **Fig. S. 2**.

Fig. S. 2: Step-by-step preparation steps of Cu NPs.

3. Preparation of the Cu-loaded nanocomposite ($Co_{0.5}Ni_{0.5}Fe_2O_4/SiO_2/TiO_2/Cu$)

The Cu NPs obtained from the method described in the previous section were uniformly distributed over the external surface of the prepared composite matrix (section 2.2.1) using a simple impregnation method. Firstly, the CNFST composite matrix (250 mg) was dispersed in super dehydrated ethanol (50 mL) via water bath sonication for 45 min. Next, the prepared Cu NPs (27.77 mg) were added into the dispersion, which was then vigorously stirred overnight. Finally, the resultant powder was collected via centrifugation, washed many times using DI water, and dried at 60°C for 2 h. **Fig. S.3** shows a schematic presentation of the preparation steps used to prepare the CNFST/Cu nanocomposite.

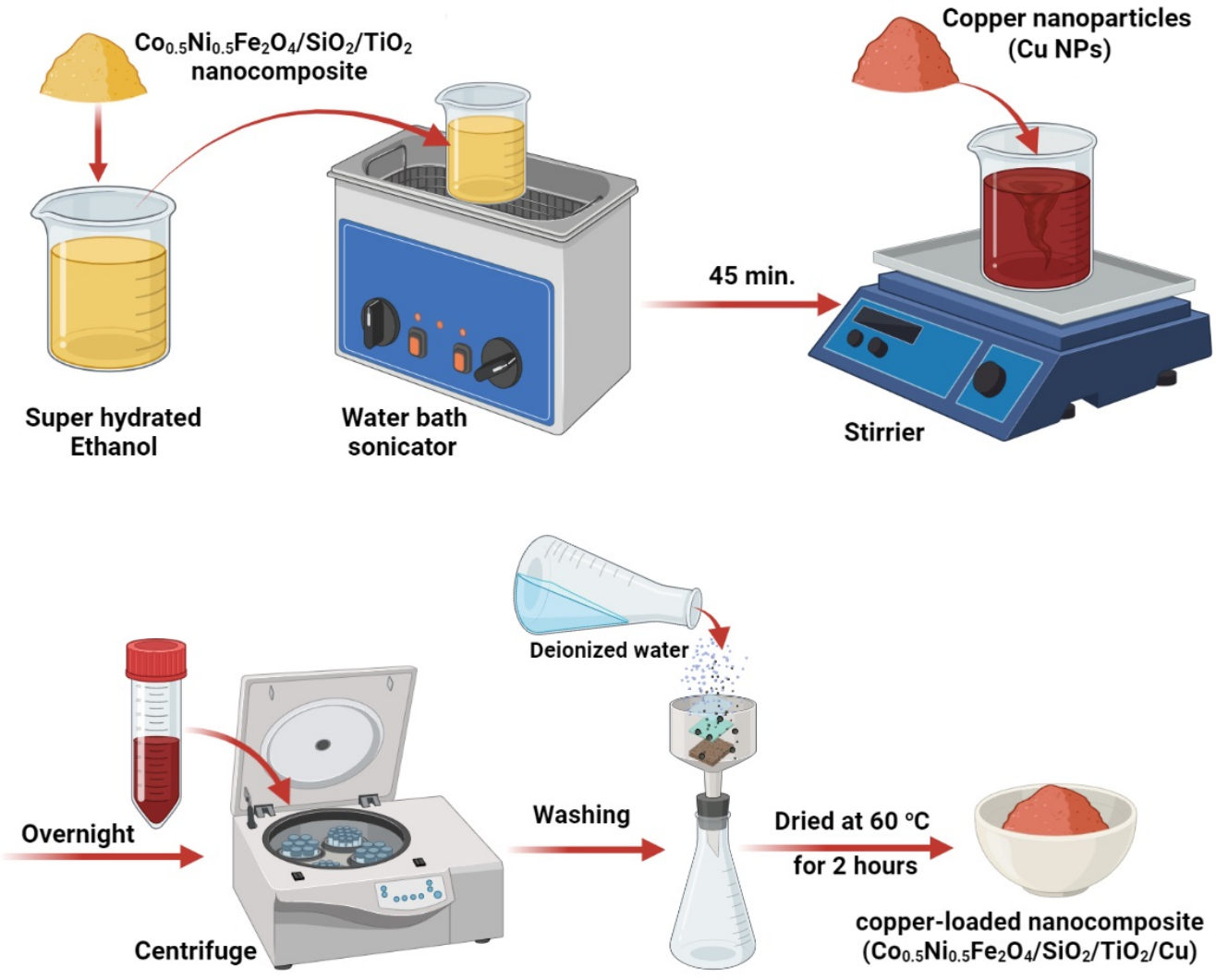

Fig. S. 3: Step-by-step preparation steps of CNFST/Cu nanocomposite.

4. Photocatalytic degradation assessment

Photocatalytic removal of aqueous solutions of potassium permanganate and pNA was carried out at ambient temperature (25°C ± 2°C). Initially, a fixed quantity of each sample was mixed with known volume and fixed initial concentration of dyes at a determined pH value. For Photolysis evaluation, tested pollutants were irradiated with UV light over time without photocatalysts. While for removal efficiencies due to adsorption, no UV light was used. Finally, for the photocatalysis experiments of potassium permanganate and pNA, suspensions were stirred for 2 h in the dark until adsorption–desorption equilibrium was reached. Then, suspensions were irradiated under a 10 W high pressure mercury lamp with a mean wavelength of 254 nm. After that, at fixed time intervals (10 min), the supernatant (2 mL) was sampled using a filter-supported syringe (2.5 μm filter pore size). Then, the filtered supernatant was further purified via centrifugation at 7000 rpm for 12 min to eliminate any remaining photocatalyst particles. Eventually, the change in the concentration of the dyes during photodegradation was determined via liquid cuvette configuration spectroscopic UV–vis analysis from absorbance calculations at λ_{max}, in which DI water was employed as a reference for the UV–vis calculations. While for the chromium reduction experiments, 100 ppm of a stock solution of Cr (VI) was prepared by dissolving 0.0283 g of $K_2Cr_2O_7$ in 100 mL DI water. The samples (0.01 g) were dispersed in a beaker filled with Cr (VI) (20 ppm, 20 mL). The effects of pH and EDTA were studied using 1 mM of EDTA as a hole scavenger in solution at pH 2 and 5. The 1 mM of EDTA was prepared by dissolving 0.003 g of EDTA in 100 mL of Cr (IV) solution, and the pH was adjusted using H_2SO_4. The prepared samples were continuously stirred in the dark for 60 min to reach adsorption–desorption equilibrium before UV irradiation. After this, the samples were then irradiated under a TUV 54-W UVC germicidal light (Philips, illumination at 254 nm) for 2 h. Then, 1.5 mL aliquots of the sample solutions were withdrawn at different time intervals during the exposure, and the remaining concentration of Cr (VI) in the solutions was calculated using **Eq. (1)** and via UV–vis spectroscopic analysis at a wavelength of 350 nm.

$$\textbf{Cr(VI) degradation} = C_t / C_o \text{ ---------- Eq (1)}$$

where C_t is the concentration at each time interval and C_o is the initial concentration after adsorption–desorption equilibrium was reached.

5. Antimicrobial activity of the prepared samples

5.1 Well diffusion assay

The pathogenic microbial strains (bacteria and unicellular fungi) were obtained from culture collection by the Drug Microbiology Lab., NCRRT, Cairo, Egypt. t Theested microbes were *Staphylococcus aureus* (*S. aureus*), *Escherichia coli* (*E. coli*), *Pseudomonas aeruginosa* (*P. aeruginosa*), *Klebsiella pneumoniae* (*K. pneumoniae*), *Salmonella typhi* (*S. typhi*), *Proteus vulgaris* (*P. vulgaris*), *Proteus mirabilis* (*P. mirabilis*), *Candida albicans* (*C. albicans*), *and Candida tropicalis* (*C. tropicalis*). In these experiments, all of the isolated and examined microbial strains were maintained over nutrient agar slants at 4°C [4]. The well diffusion method was used to assess the antimicrobial impacts of the prepared nanocomposites according to the zone of inhibition (ZOI) against the examined bacteria and unicellular fungi, by employing the method reported by Chavez-Esquivel *et al*., [5]. Firstly, samples suspended in dimethyl sulfoxide (DMSO, 10 µg/mL) were prepared. Then, the microbial suspension was fixed and set to a standard 0.5 McFarland's concentration equal to 1–2 × 10^8 CFU/mL. After that, the tested bacteria and unicellular fungi were inoculated in a nutrient agar medium, and the 6 mm wells on the surface of the nutrient agar plate were packed with 100 µL of the prepared nanocomposites, in which DMSO was used as a negative control and amoxicillin (antibacterial standard) and Nystatin (antifungal standard) were used as positive controls. All tests were conducted in triplicate and the plates were incubated overnight at 37°C. A microbial spot with no growth was defined as a ZOI, measured in mm.

In addition, minimum inhibitory concentration (MIC) values of the samples against the employed bacterial and yeast strains were also measured using the well diffusion method according to the procedure reported by Kowalska-Krochmal *et al.* [6] The overnight incubated cultures were kept at 37°C for 2 h. Following that, the inoculum of the examined bacteria and yeast was set to a concentration of 0.5 McFarland. Then, a volume of 100 µL of McFarland's bacterial suspension was injected into the nutrient agar medium plates. The prepared nanocomposites were serially diluted two-fold using DMSO to various concentrations (µg/mL) and were then separately added to the 6 mm wells on the surface of the inoculated agar plates, which were then incubated overnight at 37°C. The MIC values were determined as the minimum concentration of the nanocomposites that hinder the growth of bacteria and yeast after overnight incubation.

5.2 Growth curve assay

The influence that the prepared nanocomposites has on the growth of *S. aureus* (the most sensitive microbe) was investigated using the growth curve assay method developed by Huang *et al.* [7] In this method, the bacterial suspension was adjusted to 0.5 McFarland (1 × 10^8 CFU/ml) in 5 mL

nutrient broth tubes. Equal volumes of the nanocomposites were then separately added to each of the test tubes. The absorbance at 600 nm of the bacterial growth after treatment was evaluated every 2 h up to 24 h. The average of duplicate readings was calculated with respect to time to obtain a regular growth curve.

5.3 Potential effect of UV activation on the antimicrobial activity of the synthesized nanocomposites

The antimicrobial potential of the prepared samples in the presence and absence of UV light was investigated against the tested pathogenic microbes (*S. aureus)* using optical density design [8]. Bacterial cultures that had been incubated for 2 h were set to a standard 0.5 McFarland (1×10^8 CFU/ml). 100 µL nanocomposite samples were mixed with the tested microbial tubes. The tubes were then divided into two groups, tubes with non-UV irradiated nanocomposites and tubes containing nanocomposites that had been UV irradiated for 15, 30, 45, 60, and 75 min with 6.9 mW cm^{-2} intensity light. Then, the turbidity of the samples was measured at 600 nm [9]. The inhibition percentage (%) of the examined bacterial pathogens was determined using **Eq. 2**, according to the method reported by Abd Elkodous *et al*. [10]

$$Inhibition\ \% = \frac{ODc - ODt}{ODc} \times 100\ (Eq.2)$$

where ODc is the absorbance of a control sample that had not been subjected to any treatment and ODt is the absorbance of the treated samples.

5.4 Effect of the synthesized nanocomposites on protein leakage from bacterial cell membranes

Pure bacterial cells (100 µL) that had been cultured for 18 h and set at 0.5 McFarland (1×10^8 CFU/ml) were injected into nutrient broth (10 mL) containing well-sonicated and dispersed composite samples of various concentrations (0.125, 0.25, 0.5, and 1 mg/mL). Nanocomposite-free broth injected with cultured cells was used as a control. All samples were incubated at 37°C for 5 h before being centrifuged for 15 min at 5500 rpm [11]. For all of the samples, supernatant (100 µL) combined with Bradford reagent (1 mL) was analyzed. The optical densities of the samples were measured at 595 nm after 10 min of incubation in the dark [11].

5.5 Reaction mechanism estimation by SEM analysis of bacterial cells

Bacterial cells (*S. aureus*) were rinsed with phosphate buffered saline (PBS) and fixed with 3.5% glutaraldehyde. After that, the fixed cells were washed repeatedly with PBS and rinsed with ethanol for 20 min at 27°C before being dried. Finally, the *S. aureus* cells were attached to

aluminum stumps to carry out SEM observations [8]. Morphological and surface characteristics of the composite-treated and control (untreated) *S. aureus* cells were analyzed [10, 12].

6. Statistical analysis

Statistical examination of the obtained data was conducted using one-way analysis of variance (ANOVA) (at $P < 0.05$) with Duncan's multiple series and least significant difference analyses [13]. In addition, the data were examined using the SPSS software, version 15.

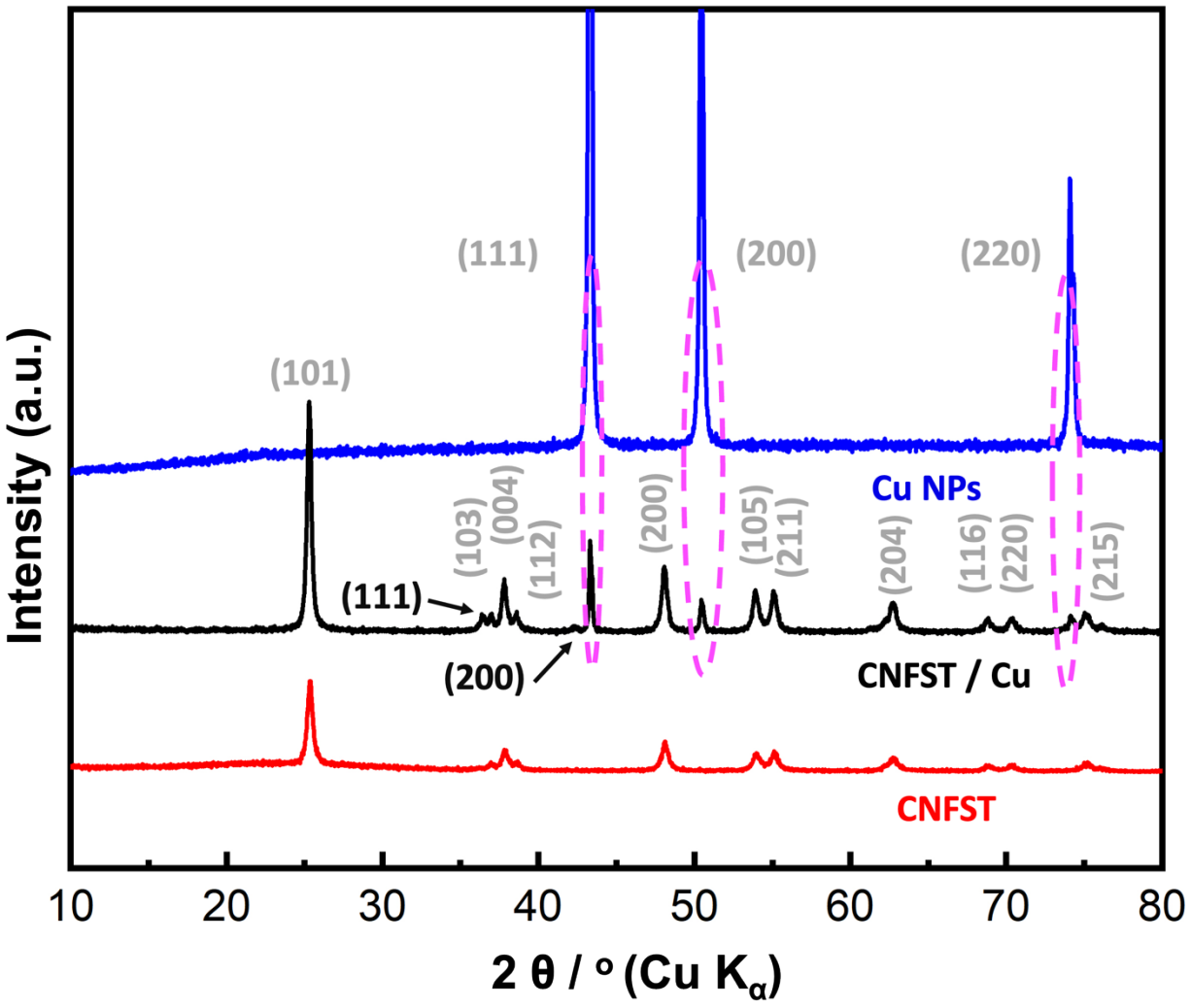

Fig. S. 4: XRD θ-2θ patterns of the prepared samples.

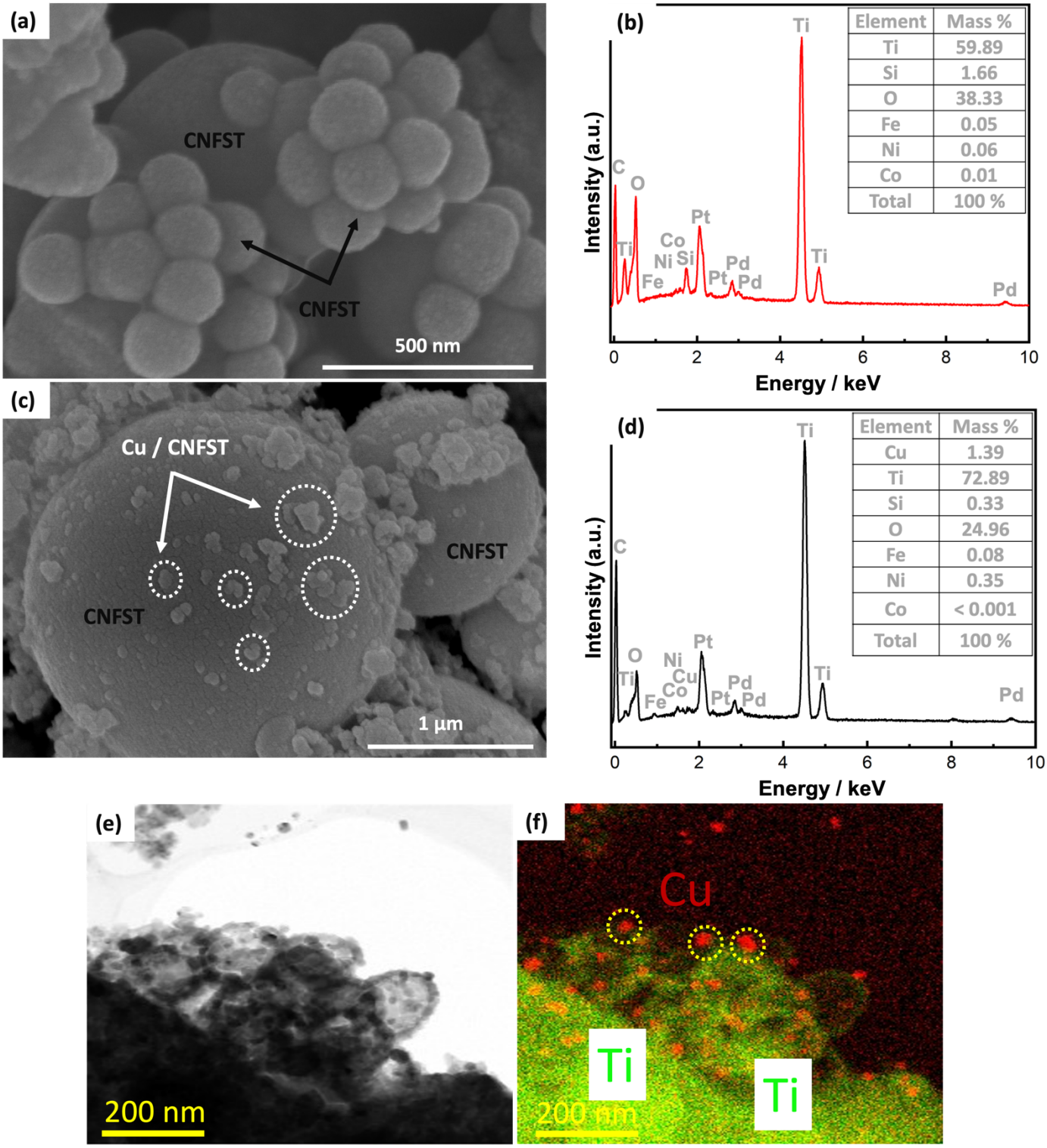

Fig. S. 5: SEM, EDX, and STEM mapping analyses of the prepared CNFST composite matrix, and CNFST / Cu nanocomposite.

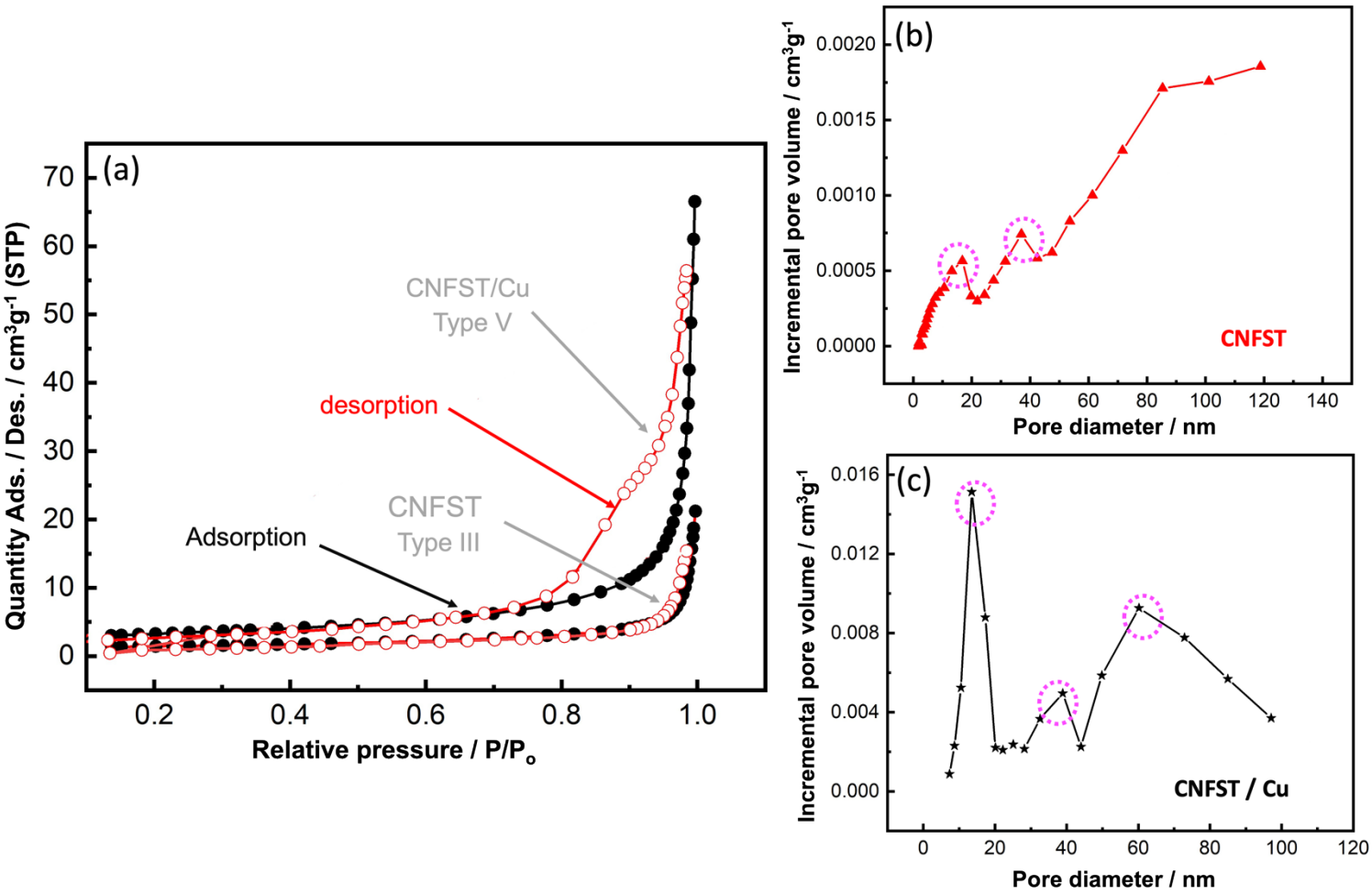

Fig. S. 6: a) N_2 adsorption-desorption isotherms, b) CNFST BJH pore size distribution, and c) CNFST/ Cu BJH pore size distribution.

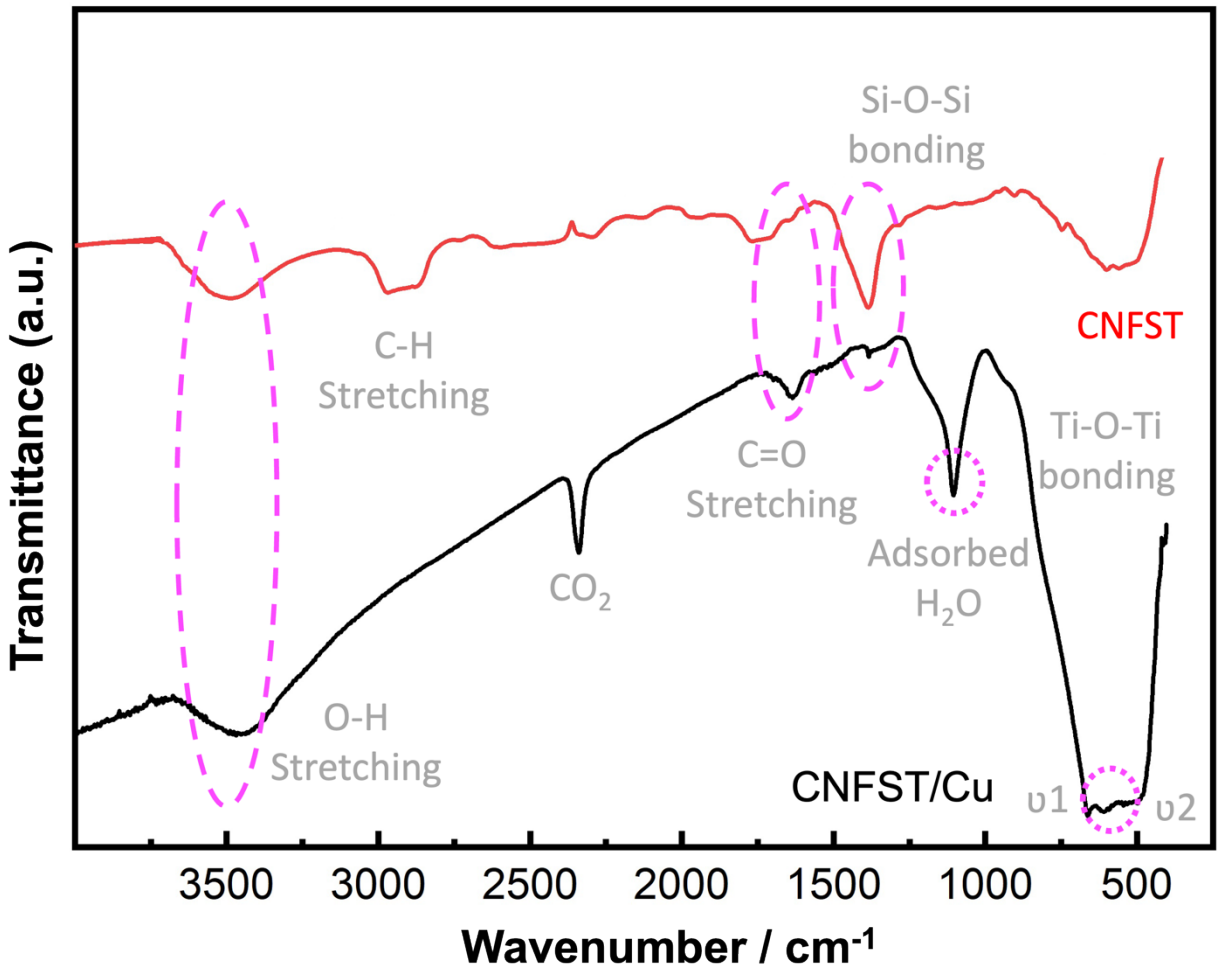

Fig. S. 7: FTIR spectra of bare CNFST matrix and CNFST/Cu 10% nanocomposite.

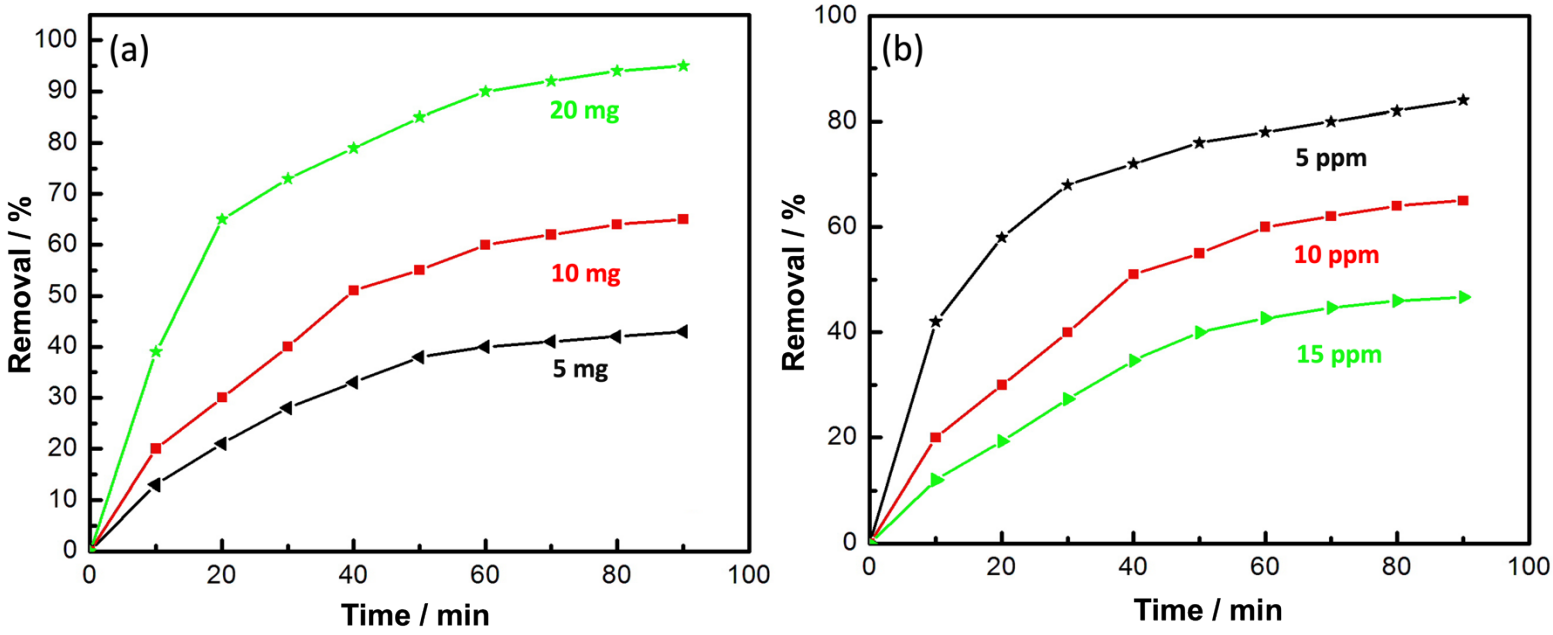

Fig. S. 8: a) Photocatalyst dose effect and b) initial pNA concentration impact on the photocatalytic performance of CNFST/ Cu photocatalyst.

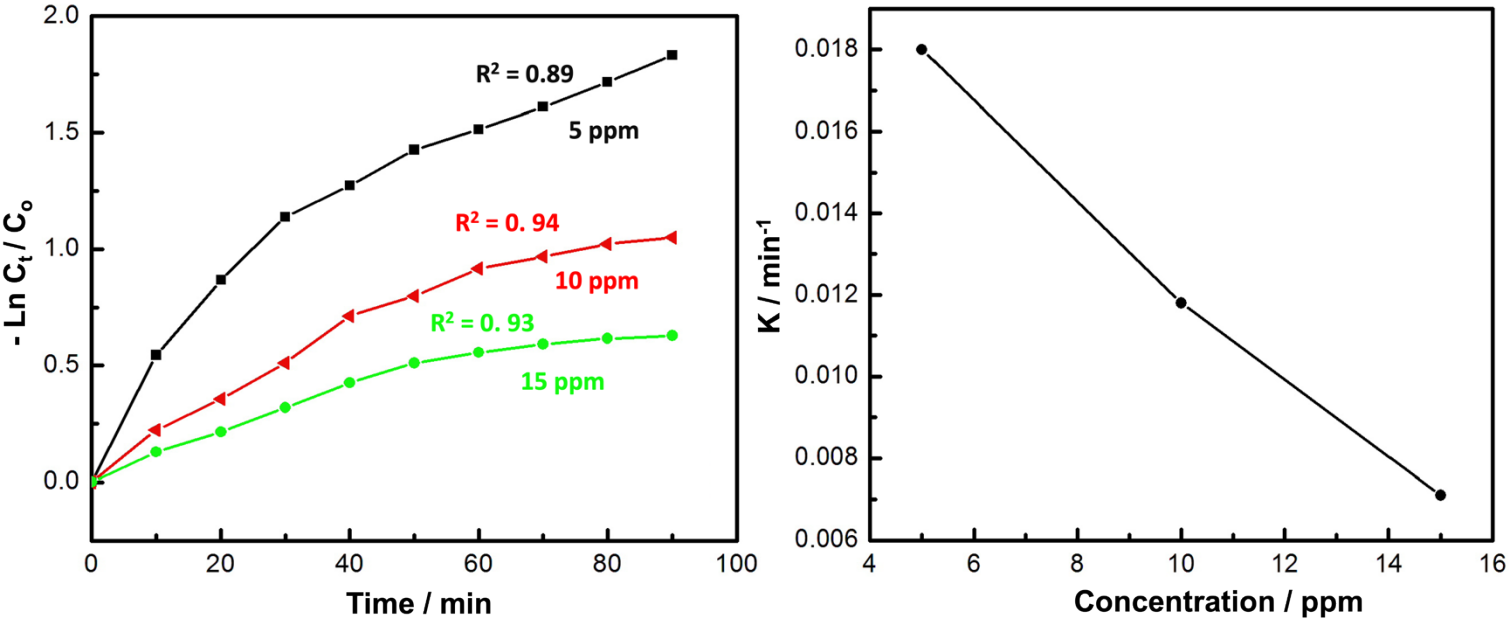

Fig. S. 9: a) Pseudo first-order kinetics plots and b) variation of apparent rate constant (k) with pNA concentration.

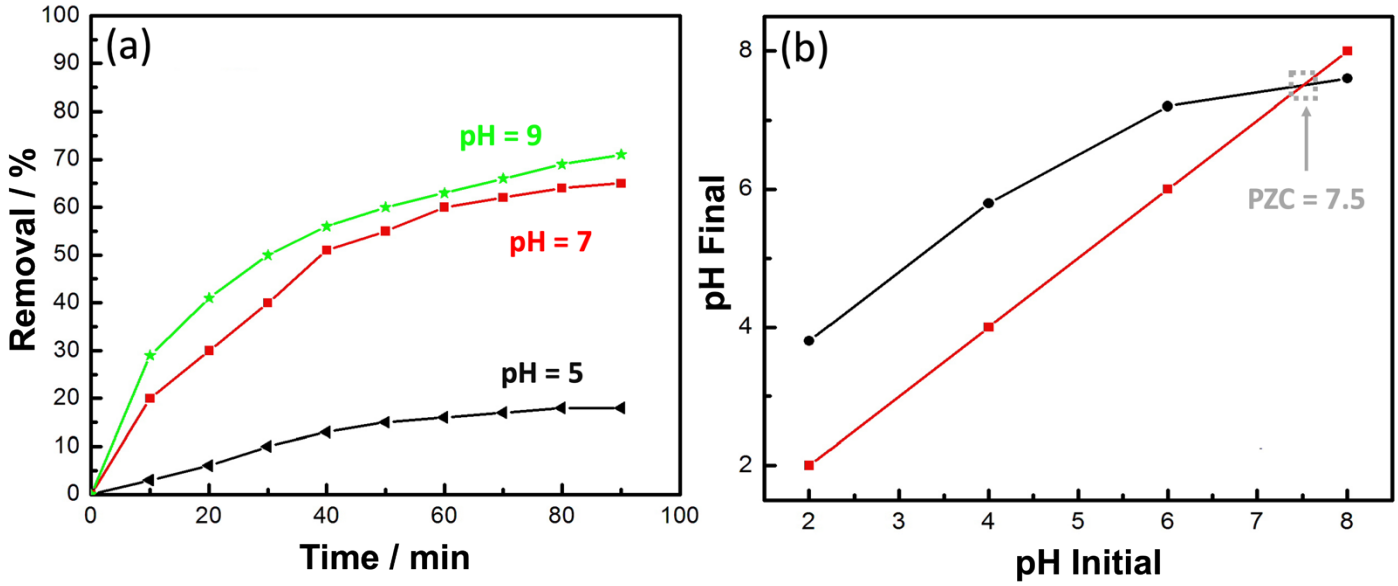

Fig. S. 10: a) Effect of pH on the removal percentage of pNA and b) PZC calculation.

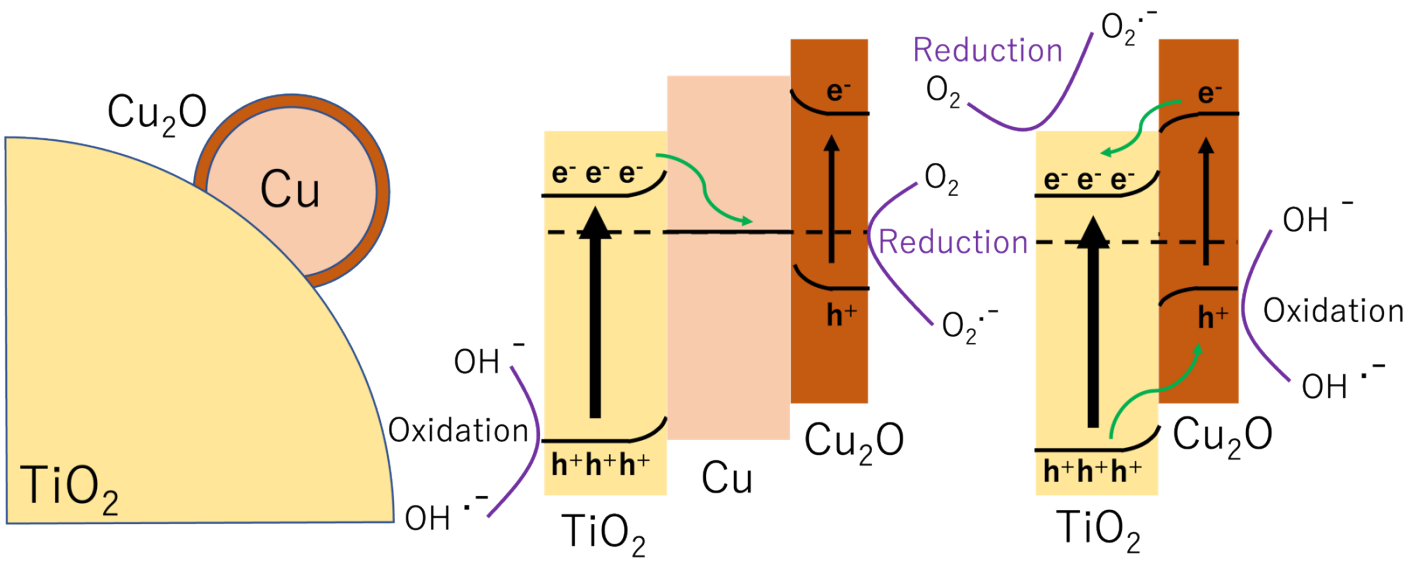

Fig. S. 11: Proposed photocatalytic reaction mechanisms over the surface of CNFST/Cu photocatalyst.

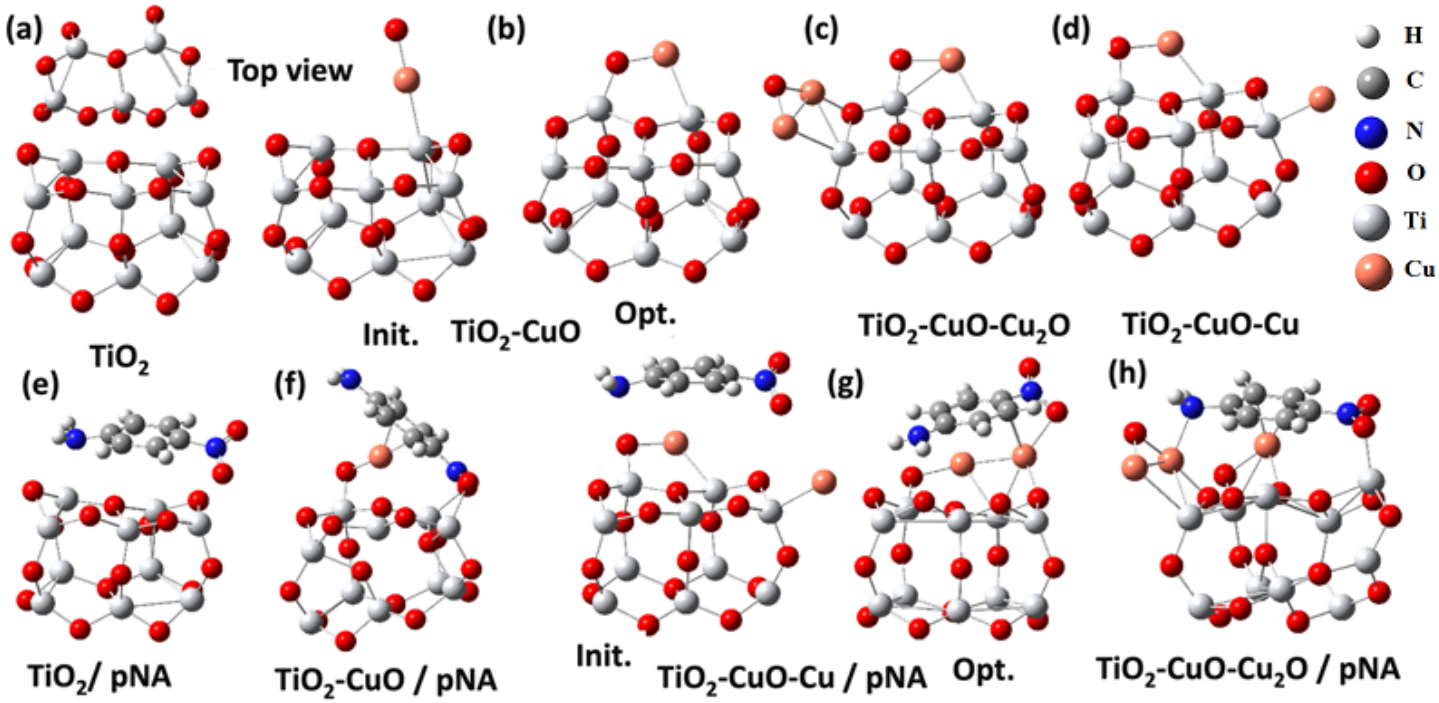

Fig. S. 12: (a) The optimized structure of TiO_2 nanoflake, (b-d) the optimized structure of TiO_2 after adding CuO, Cu_2O, and Cu. (e-h) adsorption of pNA on the previous structures. (b) and (g) shows the difference between the Initial structure (init.) and the optimized structutre (opt.).

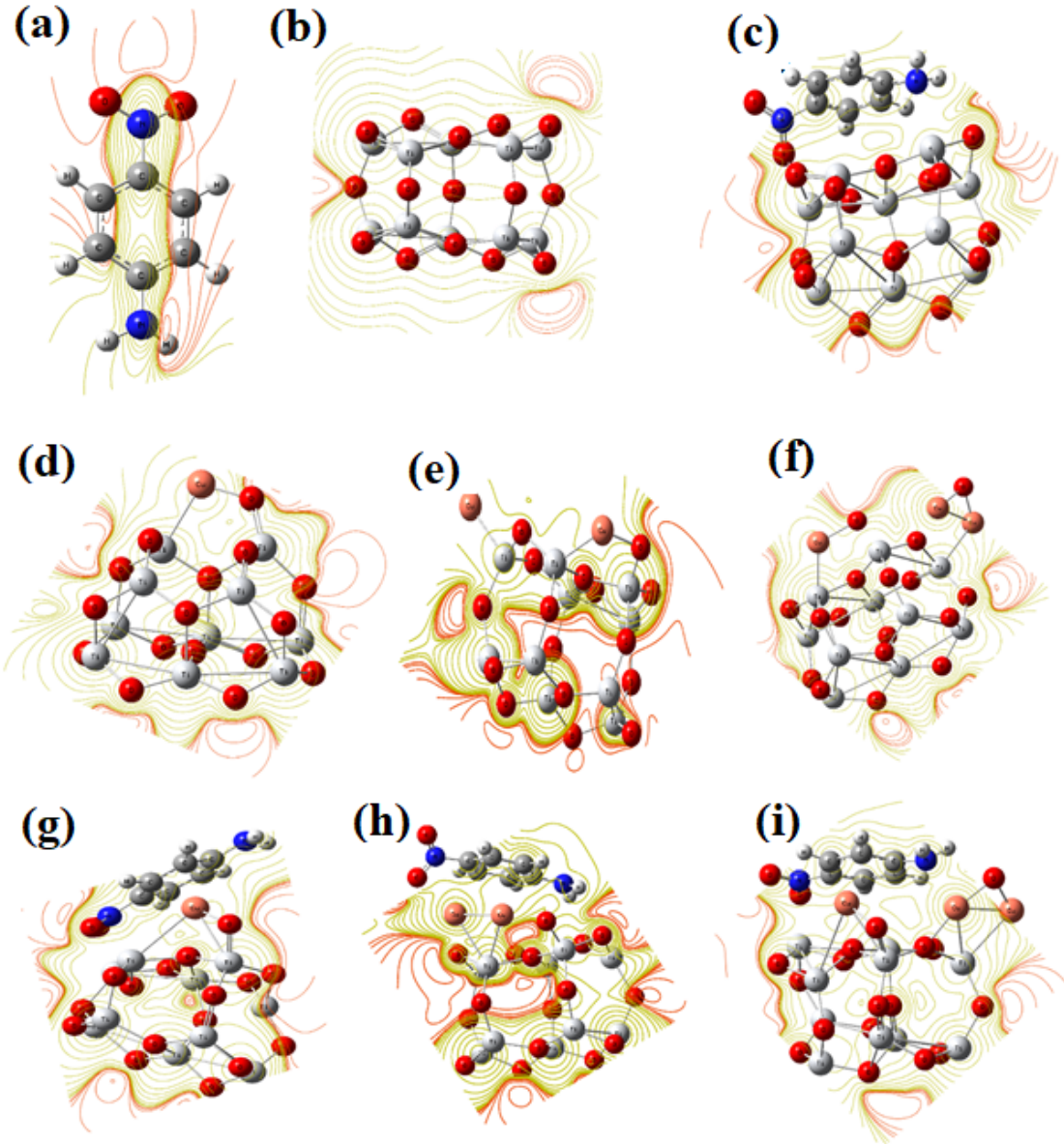
(a)
(b)
(c)
(d)
(e)
(f)
(g)
(h)
(i)

Fig. S. 13: DFT: M062X/6-31g (d, p) MESP mapping as contour for a) pNA, b)TiO_2, c) TiO_2/pNA, d) TiO_2-CuO, e) TiO_2-CuO-Cu, f) TiO_2-CuO-CuO_2, g) TiO_2-CuO/pNA, h) TiO_2-CuO-Cu/pNA, and i) TiO_2-CuO-CuO_2/pNA.

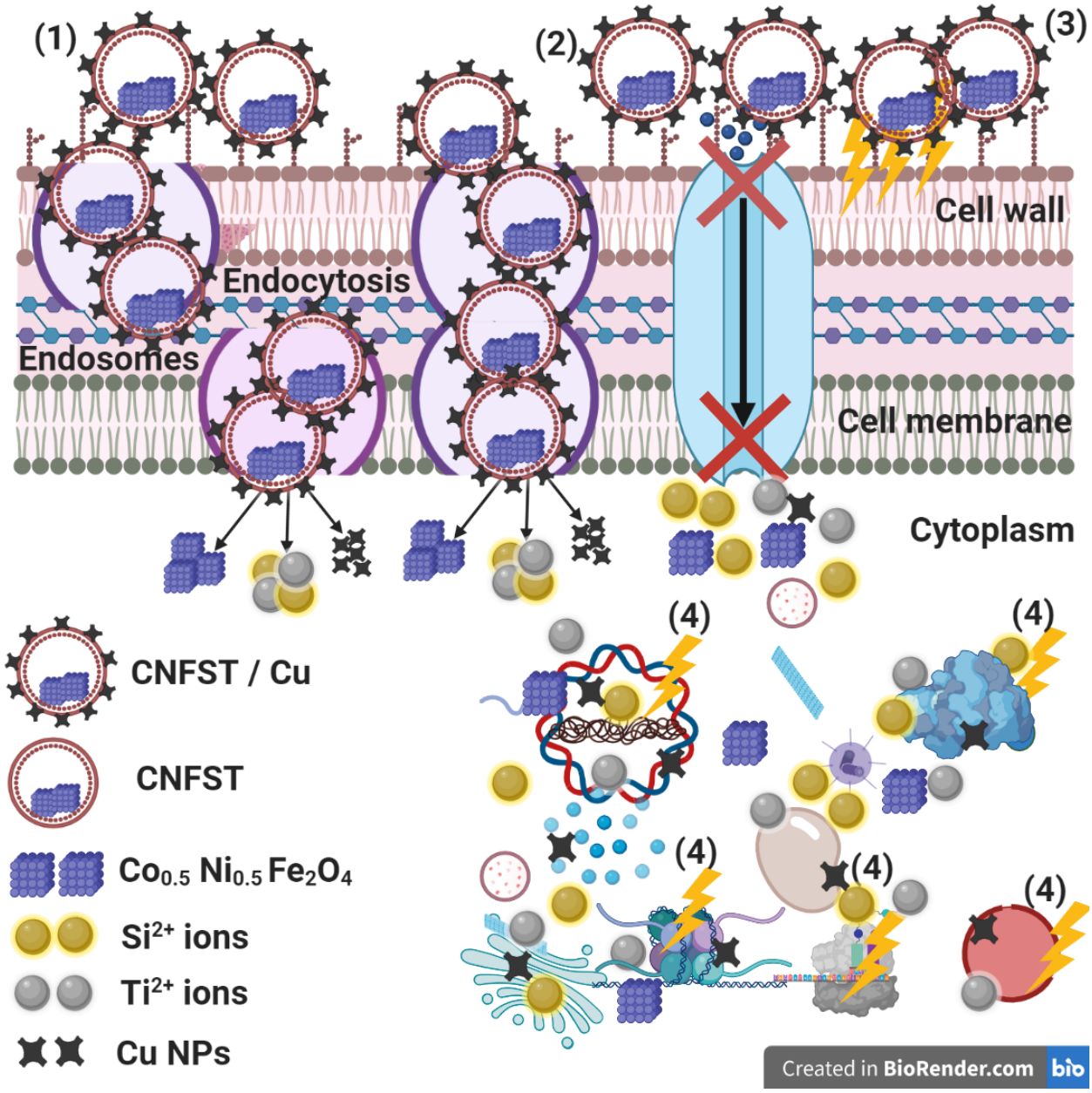

Fig. S. 14: Schematic representation of the four prominent routes of the antibacterial activity of CNFST/Cu nanocomposite, 1) nanocomposite adherence to the bacterial cell surface leading to membrane damage and switching off its transport activity, 2) nanocomposite blocking the ions transport from and to the bacterial cell, 3) ROS creation leading to bacterial cell wall damage, and 4) nanocomposite penetrates the bacterial cells and interact with their cellular organelles and biomolecules, affecting their cellular machinery, and modulating the cellular signaling system causing cell death. The prepared nanocomposite may serve as a vehicle to effectively-deliver Ti^{2+}, and Si^{2+} ions (from its outer shells) to the bacterial cytoplasm and membrane, where proton motive force would decrease the pH to be less than 3 facilitating the antimicrobial activity of Cu NPs and ferrites.

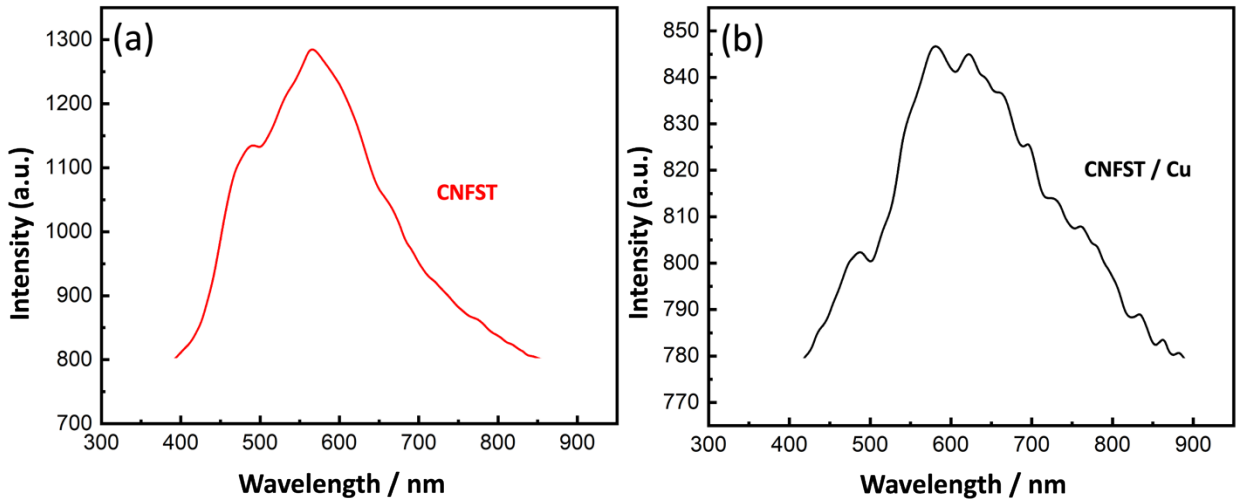

Fig. S. 15: PL spectra of a) CNFST and b) CNFST/Cu nanocomposites.

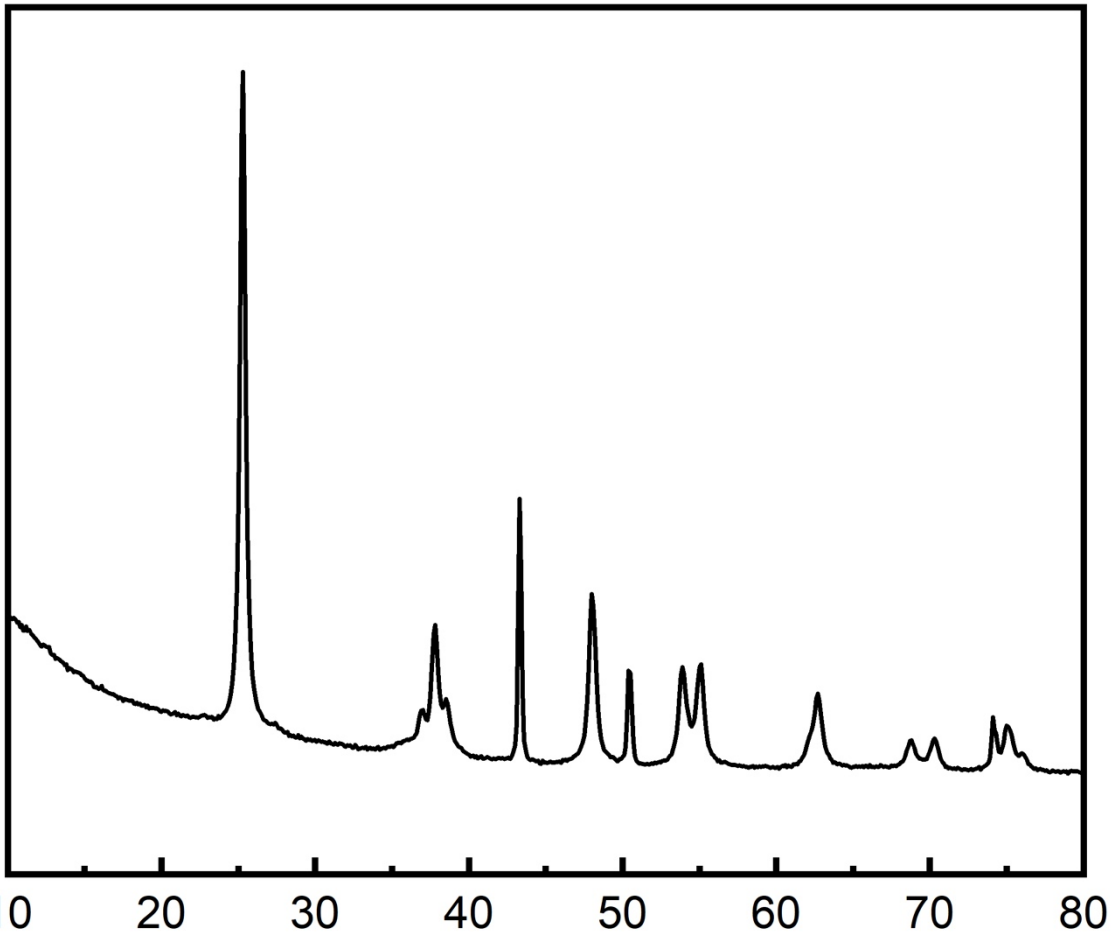

Fig. S.16: XRD analysis of CNFST/Cu sample after potassium permanganate degradation.

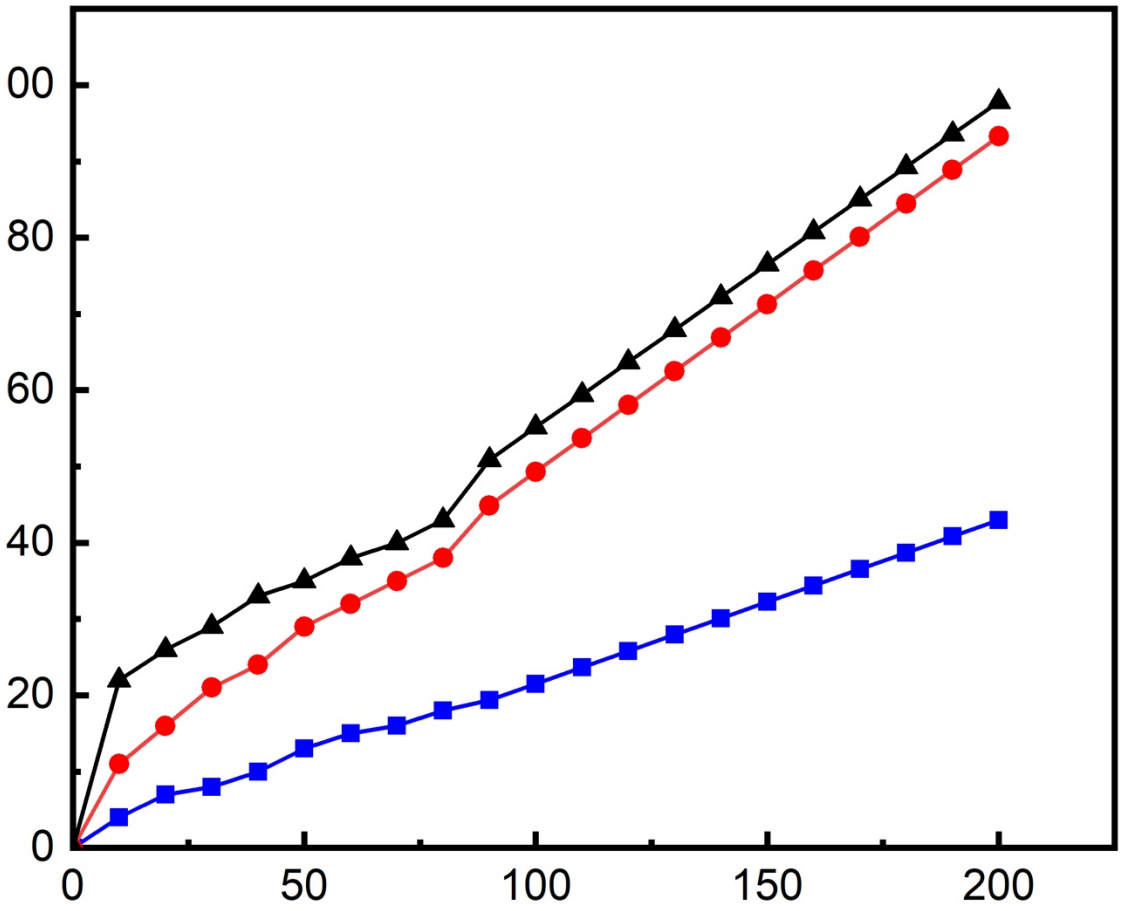

Fig. S. 17: Potassium permanganate degradation by the prepared samples after 200 min of UV irradiation (100 mg photocatalyst, 75 ml Vol., 100 ppm dye Conc., and pH =7). (Black line: CNFST/Cu, Red line: CNFST, and blue line: Cu NPs).

Table S.1: The photocatalytic degradation of pNA over some reported TiO_2-based photocatalysts.

Photocatalyst	pNA dye Conc. (mg/L)	Light type	Degradation Efficiency	Ref.
TiO_2@Au@C hollow spheres	5	Visible light	92.65% after 180 min	[14]
CdS/TiO_2	10	Visible light	98.6% after 12 h	[15]
Ag-TiO_2	30	UV radiation	81% after 2 h	[16]
$H_3PW_{12}O_{40}/TiO_2$	10	UV radiation	88.68% after 120 min	[17]
TiO_2-coated cenospheres	25	Solar light irradiation	26% after 3 h	[18]
CNFST/Cu nanocomposite	10	UV radiation	65% after 90 min	This work

References:

1. Abd Elkodous, M., et al., *Layer-by-layer preparation and characterization of recyclable nanocomposite (Co x Ni 1− x Fe 2 O 4; X= 0.9/SiO 2/TiO 2).* Journal of Materials Science: Materials in Electronics, 2019. **30**(9): p. 8312-8328.
2. El-Sayyad, G.S., et al., *Merits of photocatalytic and antimicrobial applications of gamma-irradiated CoxNi1−xFe2O4/SiO2/TiO2; x = 0.9 nanocomposite for pyridine removal and pathogenic bacteria/fungi disinfection: implication for wastewater treatment.* RSC Advances, 2020. **10**(9): p. 5241-5259.
3. Jia, X., J. Li, and E. Wang, *One-pot green synthesis of optically pH-sensitive carbon dots with upconversion luminescence.* Nanoscale, 2012. **4**(18): p. 5572-5575.
4. Abd Elkodous, M., et al., *Fabrication of ultra-pure anisotropic zinc oxide nanoparticles via simple and cost-effective route: implications for UTI and EAC medications.* Biological trace element research, 2020. **196**(1): p. 297-317.
5. Chavez-Esquivel, G., et al., *Antimicrobial activity of graphite oxide doped with silver against Bacillus subtilis, Candida albicans, Escherichia coli, and Staphylococcus aureus by agar well diffusion test: Synthesis and characterization.* Materials Science and Engineering: C, 2021. **123**: p. 111934.
6. Kowalska-Krochmal, B. and R. Dudek-Wicher, *The minimum inhibitory concentration of antibiotics: Methods, interpretation, clinical relevance.* Pathogens, 2021. **10**(2): p. 165.

7. Huang, W., et al., *Chemical analysis and in vitro antimicrobial effects and mechanism of action of Trachyspermum copticum essential oil against Escherichia coli.* Asian Pacific journal of tropical medicine, 2017. **10**(7): p. 663-669.
8. El-Shazly, A.N., et al., *Superior visible light antimicrobial performance of facet engineered cobalt doped TiO 2 mesocrystals in pathogenic bacterium and fungi.* Scientific reports, 2021. **11**(1): p. 1-14.
9. Maksoud, M.A., et al., *Gamma irradiation-assisted synthesis of PANi/Ag/MoS2/LiCo0. 5Fe2O4 nanocomposite: Efficiency evaluation of photocatalytic bisphenol A degradation and microbial decontamination from wastewater.* Optical Materials, 2021. **119**: p. 111396.
10. Abd Elkodous, M., et al., *Carbon-dot-loaded Co x Ni 1− x Fe 2 O 4; x= 0.9/SiO 2/TiO 2 nanocomposite with enhanced photocatalytic and antimicrobial potential: An engineered nanocomposite for wastewater treatment.* Scientific Reports, 2020. **10**(1): p. 1-22.
11. Agarwal, H., et al., *Eco-friendly synthesis of zinc oxide nanoparticles using Cinnamomum Tamala leaf extract and its promising effect towards the antibacterial activity.* Journal of Drug Delivery Science and Technology, 2019. **53**: p. 101212.
12. Elbasuney, S., et al., *Promising antimicrobial and antibiofilm activities of reduced graphene oxide-metal oxide (RGO-NiO, RGO-AgO, and RGO-ZnO) nanocomposites.* RSC Advances, 2021. **11**(42): p. 25961-25975.
13. Brown, A.M., *A new software for carrying out one-way ANOVA post hoc tests.* Computer methods and programs in biomedicine, 2005. **79**(1): p. 89-95.
14. Cai, J., et al., *Synergistic effect of double-shelled and sandwiched TiO2@ Au@ C hollow spheres with enhanced visible-light-driven photocatalytic activity.* ACS Applied Materials & Interfaces, 2015. **7**(6): p. 3764-3772.
15. Hu, Z., et al., *New insight into an efficient visible light-driven photocatalytic organic transformation over CdS/TiO2 photocatalysts.* Photochemical & Photobiological Sciences, 2018. **17**(1): p. 51-59.
16. Mirkhani, V., et al., *Photodegradation of aromatic amines by Ag-TiO2 photocatalyst.* Journal of the Iranian Chemical Society, 2009. **6**(4): p. 800-807.
17. Huang, W.H. and R. Liu. *Photocatalytic degradation of p-Nitroaniline with composite photocatalyst H3P12W40/TiO 2*. in *Advanced Materials Research*. 2011. Trans Tech Publ.
18. Surolia, P.K., R.J. Tayade, and R.V. Jasra, *TiO2-Coated Cenospheres as Catalysts for Photocatalytic Degradation of Methylene Blue, p-Nitroaniline, n-Decane, and n-Tridecane under Solar Irradiation.* Industrial & Engineering Chemistry Research, 2010. **49**(19): p. 8908-8919.